Solid Freeform Fabrication 2017: Proceedings of the 28th Annual International Solid Freeform Fabrication Symposium – An Additive Manufacturing Conference
Reviewed Paper

MECHANICAL PROPERTIES OF 304L METAL PARTS MADE BY LASER-FOIL-PRINTING PROCESS

Chia-Hung Hung, Yiyu Shen, Ming Leu, and Hai-Lung Tsai

Department of Mechanical and Aerospace Engineering, Missouri University of Science and Technology, Rolla, MO, USA 65409

Abstract

Laser-Foil-Printing (LFP) is a novel laminated object manufacturing process for metal additive manufacturing. It fabricates three-dimensional metal parts by using a dual-laser system to weld and cut metal foils layer by layer. A main advantage of LFP is the higher cooling rate compared to powder-based laser additive manufacturing processes due to the thermal conductivity difference between foil and powder. This study focuses on the mechanical properties of 304L stainless steel parts built by the LFP process. The experimental results indicate that the yield strength and ultimate tensile strength of LFP fabricated 304L SS parts are higher by 9% and 8% in the longitudinal direction, and 24% and 25% in the transverse direction, respectively, in comparison to the parts fabricated by the selective laser melting process. X-ray diffraction and electron backscattered diffraction are used to obtain the lattice structure and the grain size of the fabricated parts.

Introduction

Additive manufacturing (AM) has been widely used in the product fabrication in recent years [1]. AM provides a solution for fabricating complex-shaped parts that are too difficult to make by conventional machining processes [2]. Depending on its manufacturing mechanism, AM processes are divided into seven categories according to the ASTM F42 Committee. The seven categories are: vat photopolymerization, material jetting, binder jetting, material extrusion, powder bed fusion, sheet lamination, and directed energy deposition. Selective laser melting (SLM) is a powder bed-fusion process, Laser Engineered Net Shaping (LENS) is a directed energy deposition process, and Laminated Object Manufacturing (LOM) is a sheet lamination process. All of these processes have been used to produce metal parts [3-5]. The SLM process uses a laser beam to selectively melt the metal particles in a powder bed layer-by-layer [6]. The LENS process uses a laser beam to melt a metal powder supplied through a co-axial nozzle [7]. Due to the gaps between powder particles, pores may be generated within the metal parts quite easily during the SLM and LENS processes [8-10]. The pores could be an advantage in biomedical applications such as prosthetic devices and bone scaffolds [11-12]. However, in terms of mechanical properties, pores are weak points within a structure, as they reduce strength, form cracks, and may fail the created metal part [13]. In addition, gaps change the physical properties of metal materials. For example, because of the gaps, the thermal conductivity and cooling rate of the metal powder are relatively low compared to the bulk material [14-16].

Laminated Object Manufacturing (LOM) is one of the first commercialized AM technologies in the early 1990s. It uses the lamination of papers to create parts, layer by layer,

with polymer-based adhesive bonding and laser contour cutting. LOM can be applied to build parts from a variety of materials as long as they can be formed as tapes. Depending on the type of material lamination, the bonding strategy varies accordingly [17-18].

Laser-Foil-Printing (LFP) has been recently developed as a new laminated object manufacturing process. In this process, a three-dimensional metal part is built layer-by-layer using a dual-laser system for welding a metal foil and then cutting the cross-sectional contour for each layer. The dual-laser system consists of a continuous-wave infrared laser and an ultraviolet pulsed laser [19]. The LFP process can provide a more efficient way of producing metal parts than the SLM and LENS processes because of the difference in layer thickness: the foil thickness used in the LFP process is between 100 μm and 200 μm while the size of powder used in the SLM process is about 50 μm. More importantly, the LFP parts are stronger than those made by powder-bed-based AM processes because the cooling rate of the LFP process is higher, due to the higher thermal conductivity of foil compared to powder.

In this study, 304L stainless steel parts were built by the LFP process in an inert shielding gas environment with a dual-laser system. The mechanical properties of the fabricated parts were measured and compared with the original 304L foil, as well as 304L parts fabricated by the powder-based LENS and SLM processes. Electron backscattered diffraction was used to obtain the size and distribution of the grains of the LFP part. X-ray diffraction was used to determine the lattice structure of the 304L foil and the LFP part produced from the foil.

Experimental apparatus

2.1 Laser-foil-printing system

A laser-foil-printing system was developed and utilized to fabricate metal parts layer-by-layer under an argon shielding gas environment using a dual-laser system. The laser system consists of a continuous-wave (CW) fiber laser subsystem for welding and an ultraviolet (UV) pulsed laser subsystem for cutting, as shown schematically in Fig. 1. The CW fiber laser subsystem included a beam expander, a galvano-mirror scanner, and an F-Theta lens. The UV pulsed laser subsystem included optical reflection mirrors, a focal lens, and high-precision motor driven stages. The actual constructed LFP system is shown in Fig. 2. The CW fiber laser had a center wavelength of 1070 nm, beam quality factor M^2 of 3.04, and maximum average power output of 1000 W. The focal length of the F-Theta lens was 300 mm, and the spot size was 160 μm. The UV pulsed laser had a center wavelength of 355 nm, pulse width of 30 ns, and maximum average power output of 10 W. The focus length of the lens was 100 mm and the spot size was 40 μm. Both CW and UV laser beams focused on the foil surface for all experiments in order that they had sufficient heat to melt or ablate material.

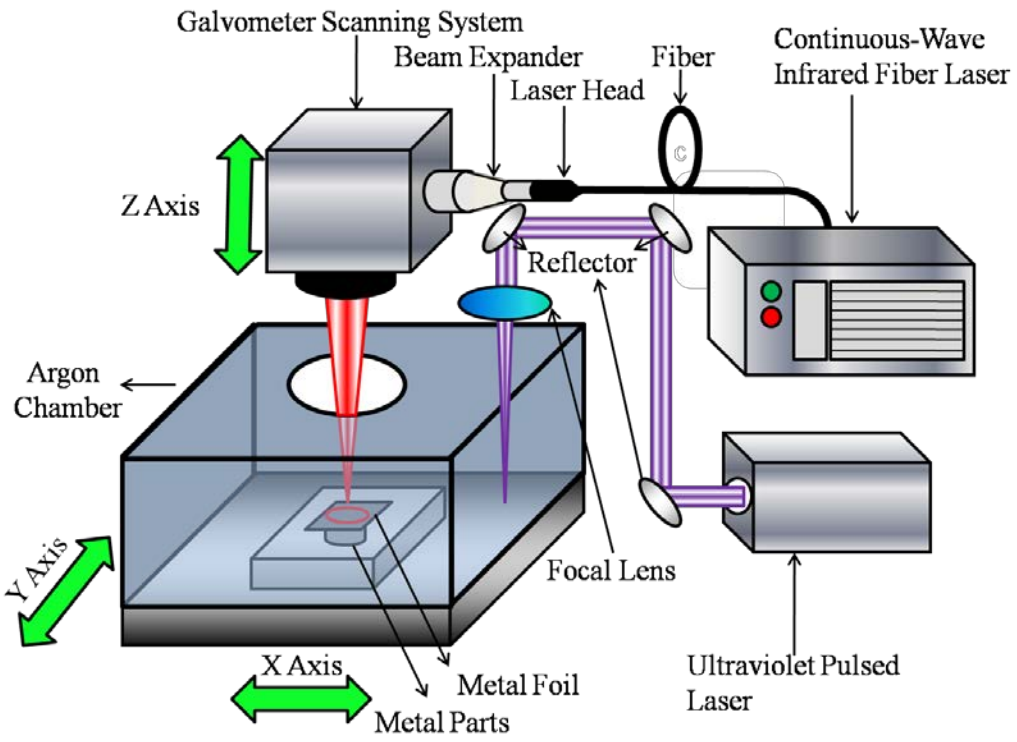

Fig. 1 Schematic illustration of the experimental setup of laser-foil-printing system

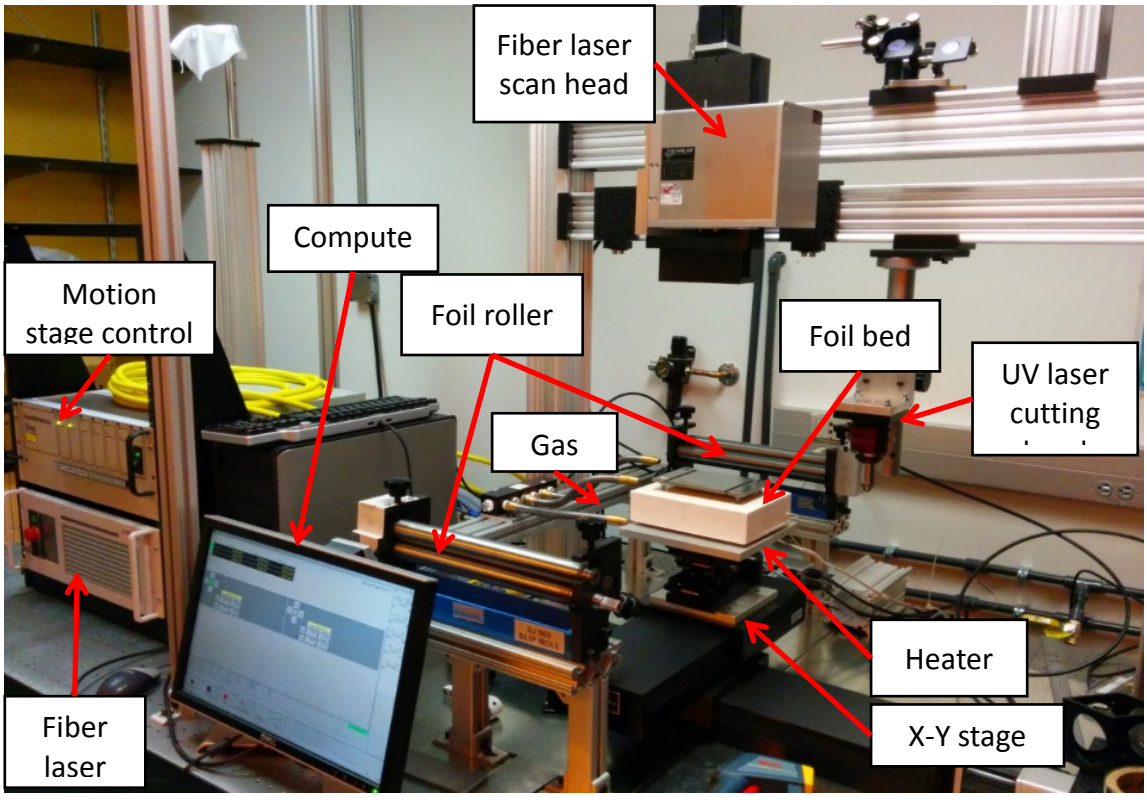

Fig.2 The constructed laser-foil-printing system

2.2 Laser-foil-printing process

To build a metal part layer-by-layer, five processing steps are followed at each layer, as illustrated in Fig. 3. First, a metal foil is transported to a specific location on the top of initially the substrate and then the metal part being fabricated, as shown in Fig. 3a. Next, spot weld is applied on the metal foil using a CW fiber laser as shown in Fig. 3b. The spot weld is used to fix the foil onto the previous layer and to prevent thermal distortion of the foil during follow-on processing. The third step is pattern welding which uses a raster scan strategy as shown in Fig. 3c. The fourth step is to cut the patterns' contour using a UV pulsed laser as shown in Fig. 3d. Finally, excess foil is removed in the fifth step as shown in Fig. 3e. A new layer is built after these five steps. In this study, for the spot welding, the CW fiber laser power was 400 W, the weld time was 0.5 ms, and the distance between spots was 1mm. For the pattern welding, the laser power was 400 W, the scan speed was 200 mm/s, and the hatch space was 0.1 mm. the UV pulsed laser used for cutting the pattern's contour had the power of 10 W and the cutting speed was 5 mm/s.

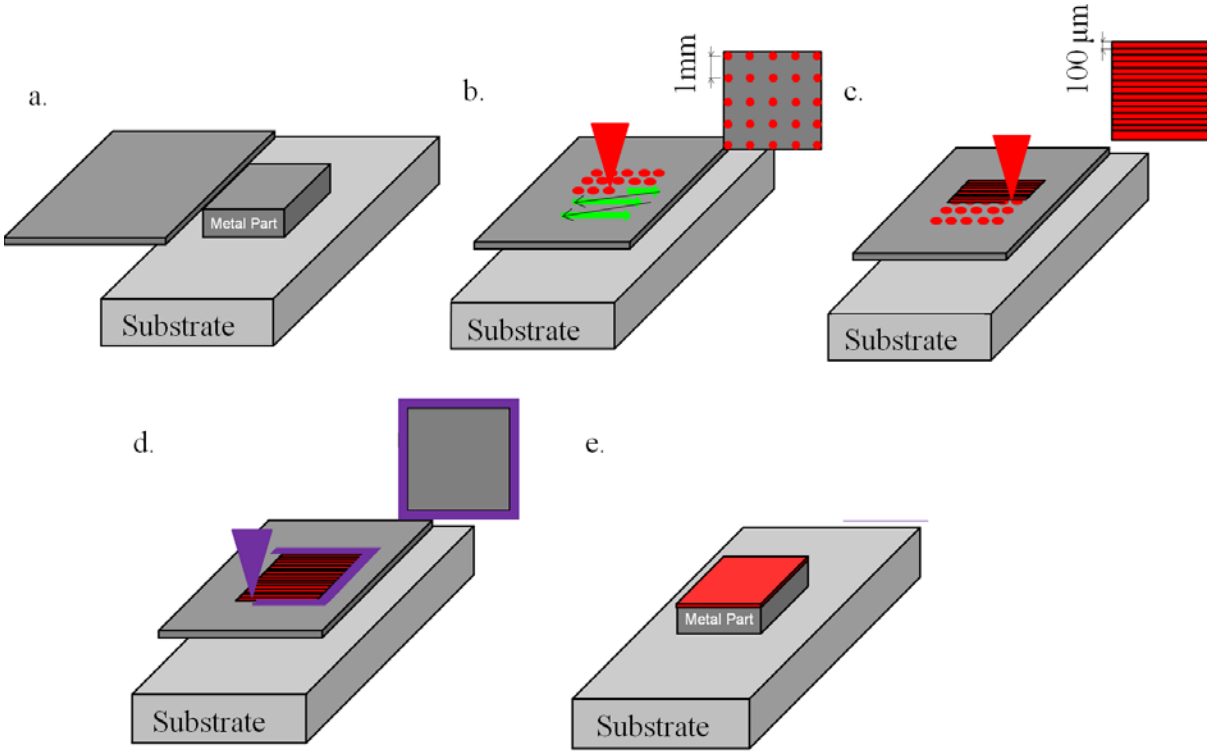

Fig. 2 Schematic illustrations of five steps performed for each layer (a) foil feeding (b) spot weld (c) pattern weld (d) contour cutting (e) excess foil removing

2.3 Experiments

The foil material used in this study was 304L stainless steel, and foil was made from annealed heat treatment. 304L SS is widely used in a variety of industrial applications since the material possesses the properties of high corrosion resistance in a harsh environment and good weldability [20]. The foil used was square in shape, with each side measuring 38.1 mm. Its thickness was 0.125 mm.

A rectangular block with the dimensions of 12 mm × 12 mm × 10 mm was built from 304L foil using the LFP process under an argon gas shielding environment. Figure 4a shows two tensile bars cut from the block, one along the layer-build direction (i.e., transverse direction, TR) and the other along the laser scanning direction (i.e., longitudinal direction, LONG), using a wire electrical discharge machining (EDM) machine. Note that the longitudinal and transverse directions are the two directions that the part has either the highest or lowest strength [23-24]. The dimensions of the bars are shown in Fig. 4b [21].

The 304L foil and the LFP part were then polished and electro-etched for observation using an optical microscope [22]. An INSTRON test frame was utilized to measure the mechanical properties of the LFP part. Hirox KH-8700 digital microscope was used to obtain the microstructure images of the 304L foil and the LFP part. A Philips X-Pert diffractometer was used to obtain X-ray diffraction pattern for determining the lattice structures of the LFP part and the 304L foil from which the part was produced. Electron backscattered diffraction was used to obtain the size and distribution of grains of the LFP part using an FEI Helios Nanolab 600 DualBeam (FIB/SEM) system.

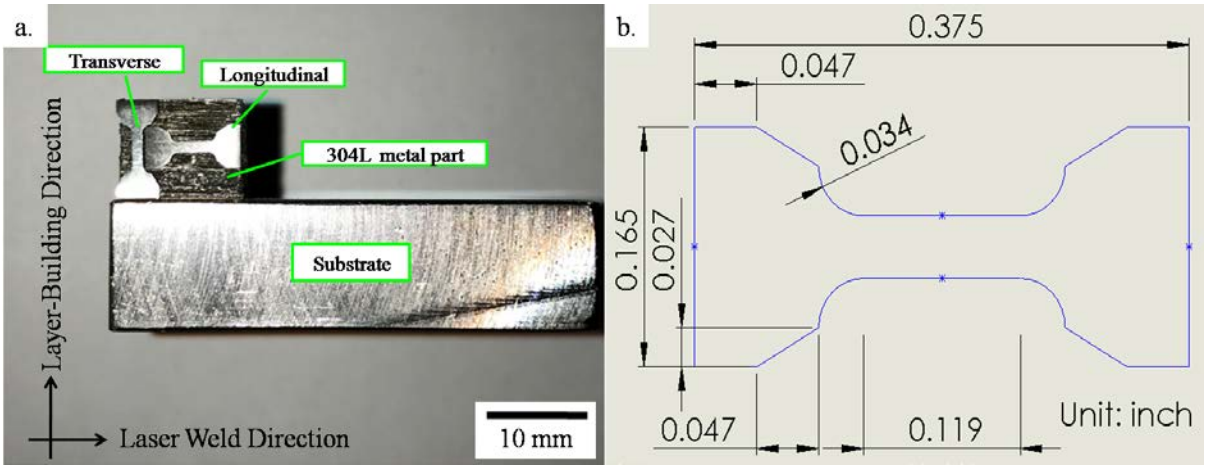

Fig. 4 (a) Side-view of the 304L metal part using laser-foil-printing process, the longitudinal and transverse tensile bars (b) dimensions of the tensile bar

Results and discussion

The test results on yield strength (YS) and ultimate tensile strength (UTS) of the 304L tensile bars compared to the YS and UTS of the 304L foil used in the LFP process are shown in Fig. 5. From the comparison of the mechanical properties of the 304L foil with the LFP part in the longitudinal (LONG) direction shows that the LFP part had 122% higher YS and 19% higher UTS compared to the metal foil. Figure 5 also shows that the 304L parts produced by the LFP process were superior to the 304L parts produced by the powder-based LENS and SLM processes in both YS and UTS [23,24]. In the longitudinal direction, the YS and UTS of the LFP parts were higher by 31% and 7%, respectively, compared to the LENS parts, and were higher by 9% and 8% compared to the SLM parts. In the transverse direction, the YS and UTS of the LFP parts were higher by 72% and 9% compared to the LENS process, and were higher by 24% and 25% compared to the SLM process. Moreover, both the YS and UTS of the LFP parts were more

uniform in both longitudinal and transverse directions in comparison to the LENS and SLM parts, as shown in Fig. 6. The YS ratio in the longitudinal vs. transverse direction was 95%, and the UTS ratio in the longitudinal vs. transverse direction was 94%, in comparison to these ratios of 72% and 92% for the LENS parts and 84% and 81% for the SLM parts. The greater uniformity in the YS and UTS of the LFP part is mainly because the bonding strength between layers is stronger in both directions for the LFP parts compared to the LENS and SLM parts.

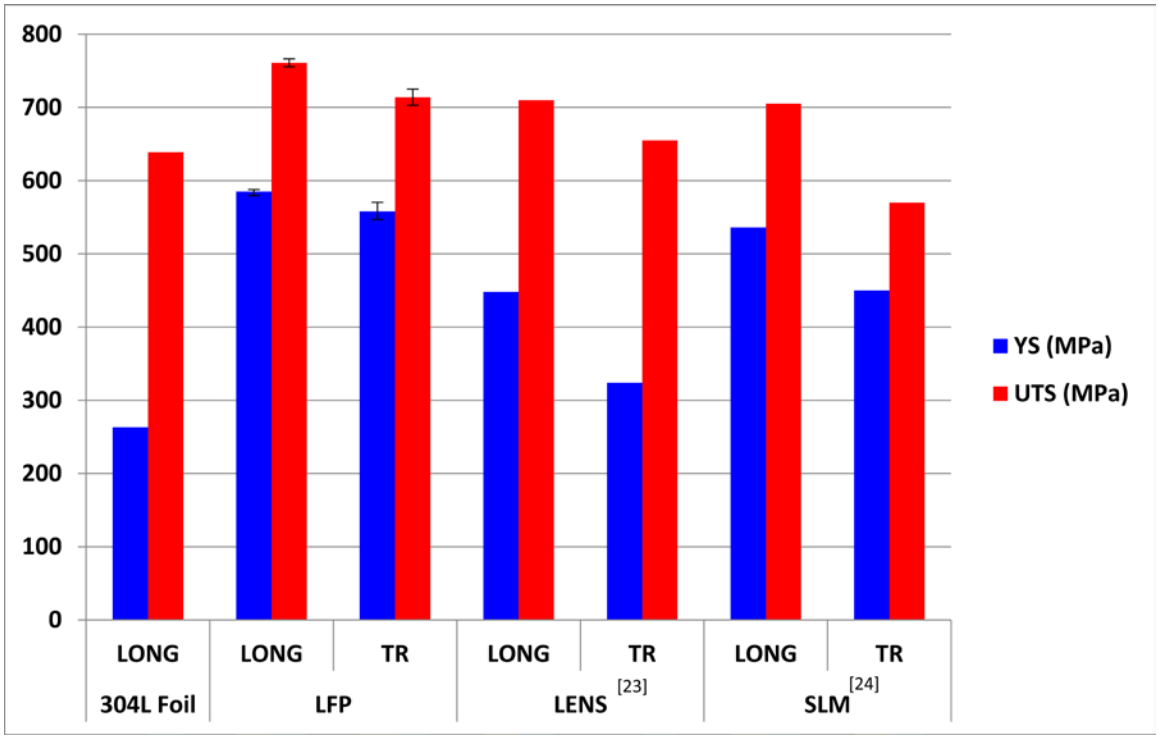

Fig. 5 Comparison of yield strength and ultimate tensile strength between the 304L foil and the parts fabricated by the LFP, LENS[23], and SLM[24] processes

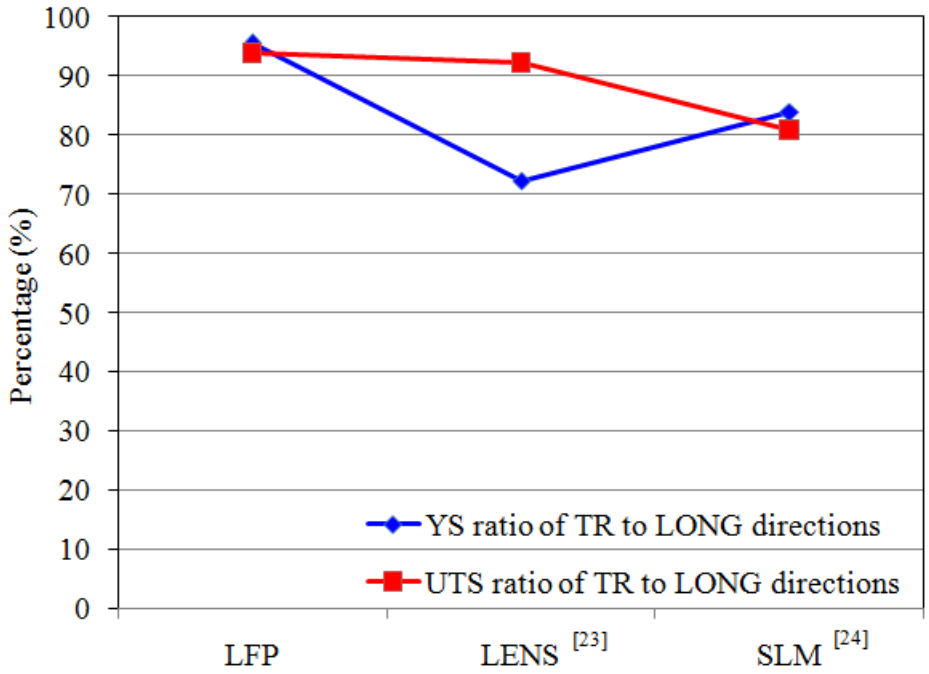

Fig. 6 The YS and UTS ratios of the transverse direction to the longitudinal direction for the LFP, LENS[23], and SLM[24] parts

Figure 7 presents the images of two breaking tensile, one along the longitudinal direction and the other along the transverse direction, using an optical microscope. Figure7a shows a typical fracture of LFP tensile bars. The broken tensile bar in Fig. 7b shows a fractured angle of 54 degrees, indicating that the 304L foils were fully melted during the LFP process, and there was remelting of the previous layer, which minimizes delamination. A typical weld pool can be seen in Fig. 8a which shows a penetration depth of 400 μm, which is more than three times of the layer thickness. The grains of the LFP part could not be observed from Fig. 8a, which shows the melt pools of laser scans using a hatch spacing of 100 μm. The illustration of a single melt pool is shown in the dashed line in this figure, from which the penetration depth and width of about 400 μm and 350 μm, respectively, can be estimated. The shape of the melt pool indicates that the laser was operating in a keyhole mode during the LFP process. Figure 8b shows the micro-structure of the foil, with the mean grain size measured ~15 μm.

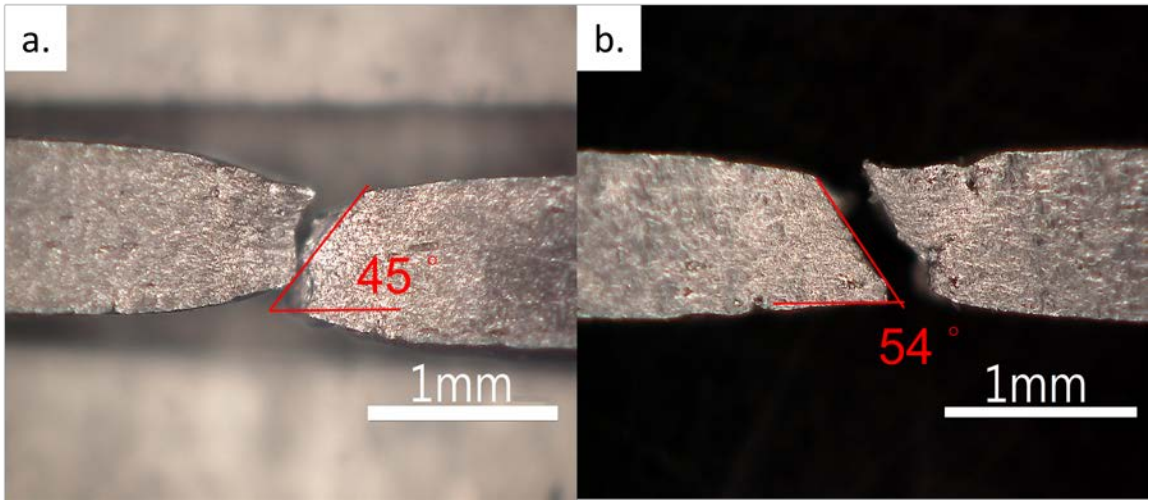

Fig. 7 Optical microscope images of the LFP tensile bars at the breaking point: (a) longitudinal direction (b) transverse direction

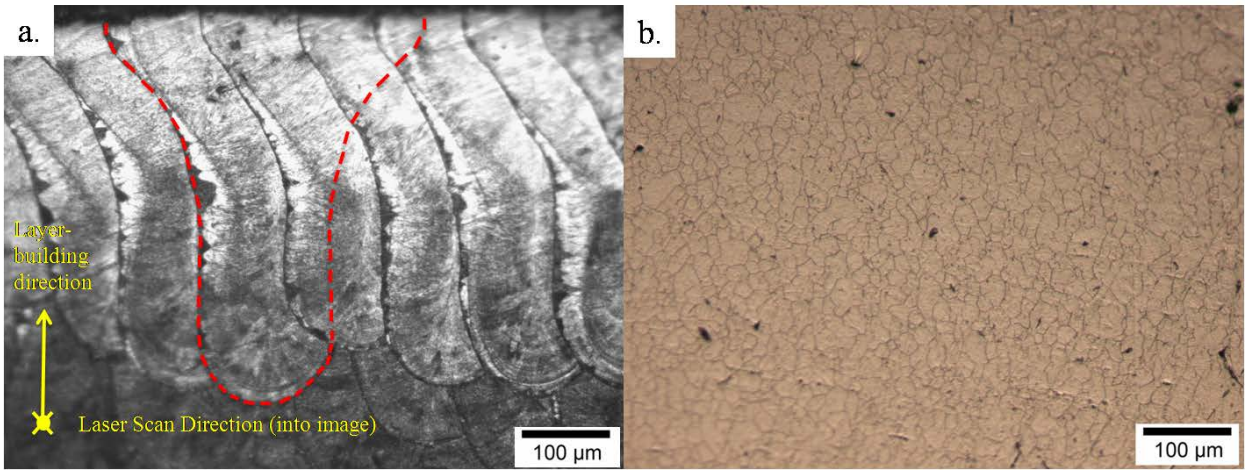

Fig. 8 Optical microscope images for (a) LFP part (b) 304L foil

Since the mean grain size of the LFP part could not be measured from Fig. 8a, electron backscattered diffraction (EBSD) was used to obtain the mean grain size of the LFP part as shown in Fig. 9. The mean grain size of the LFP part was ~3.5 µm from the distribution of 85 austenitic grains. Therefore, the grains had been refined from ~15 µm in the foil to ~3.5 µm in the LFP part. This is due to the higher cooling rate and shorter solidification time in the LFP process compared to the annealed heat treatment process for producing the metal foils [25,26].

Based on the mean grain size from the EBSD pattern, the grain refinement can be used to explain the strength enhancement in the LFP part. The yield strength could be estimated by using the Hall-Petch strengthening equation [27,28]:

$$\sigma_y = \sigma_0 + \frac{k_y}{\sqrt{d}} \tag{1}$$

where σ_y is the yield strength, σ_0 is the resistance of the lattice to dislocation motion, k_y is the strengthening coefficient, and d is the mean grain size. The Hall-Petch strengthening equation shows that (σ_y - σ_0) is inversely proportional to the square root of the mean grain size [27,28]. For 304L, σ_0 is 194 MPa and k_y is 695 MPa $m^{1/2}$ [29]. The yield strength calculated using the above equation is 565 MPa at the mean grain size of 3.5 μm. The calculated yield strength agrees well with the measured yield strength of the LFP (see Fig. 4). The finer grains of the LFP part contribute to the higher yield strength because the cooling rate of the LFP process is faster than the foil producing process and the powder-based LENS and SLM processes [23,24].

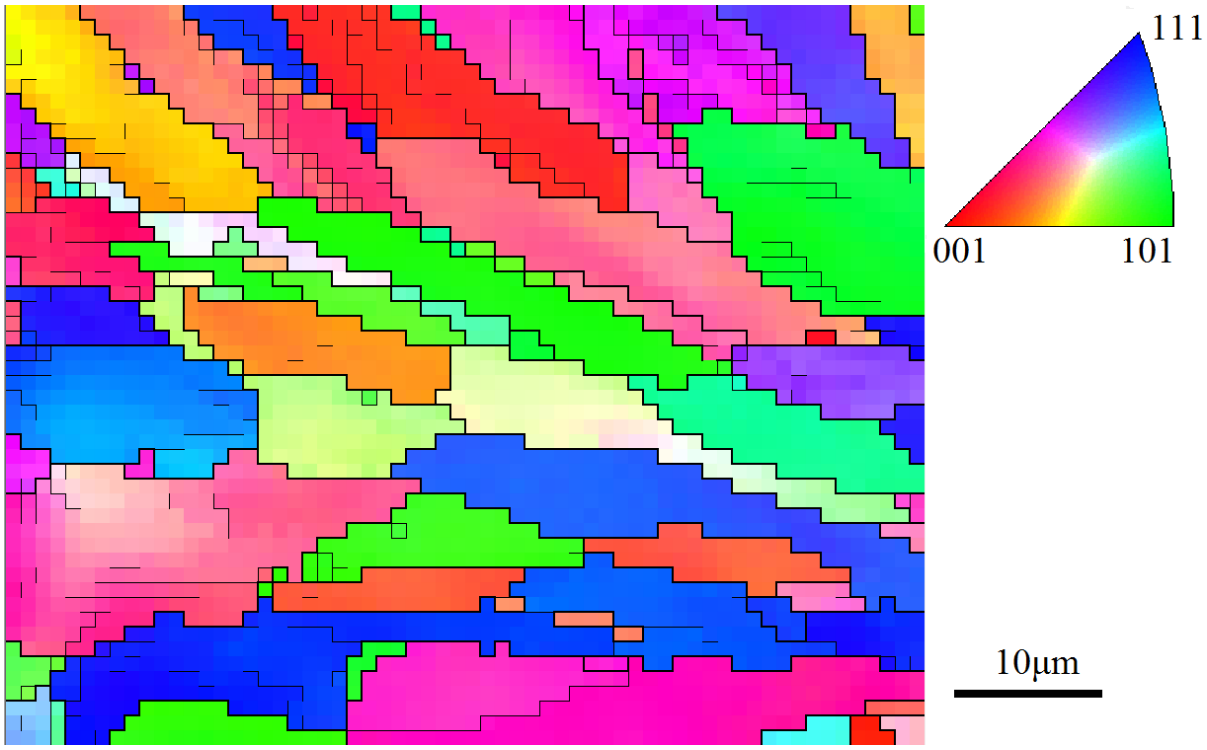

Fig. 9 EBSD pattern showing the distribution of austenitic grains with various orientations

The X-ray diffraction (XRD) patterns of the metal foil and the LFP part produced from the foil are shown in Fig. 10. Both patterns reveal austenitic phases having face-centered-cubic (FCC) structures [30]. The highest peaks of the foil and the LFP part had the orientations of (220) and (111), respectively. This difference in the orientations was due to the difference in the fabrication process. Although the foil and the LFP part both have austenitic phases, they are different types of austenitic phases. The LFP part has the metastable austenitic phase due to high cooling rate and short solidification time [31], while the foil has the equilibrium austenitic phase due to the slower cooling rate in the annealed heat treatment. The metastable austenitic phase possesses the characteristics of high strength and ductility [32].

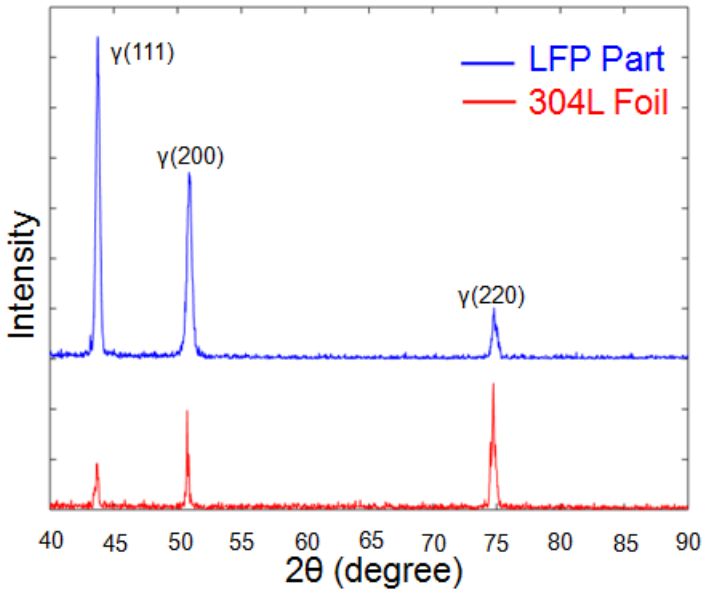

Fig. 10 X-ray diffraction patterns of the 304L foil and the LFP part

Conclusions

In this study, the mechanical properties of the 304L parts produced by the LFP process are compared to those of the 304L foil used in the LFP process and the parts produced from 304L powder by the LENS, and SLM processes. The comparison results show that the LFP part is stronger than the metal foil and the LENS and SLM parts. The higher strength of the LFP part is contributed to by the grain refinement, from the coarse grains of ~15μm to the finer grains of ~3.5μm, in the LFP part because the LFP process has a higher cooling rate than the annealed heat treatment process, LENS and SLM processes. Also, the strength of the LFP part in both longitudinal and transverse directions is more uniform than the LENS and SLM parts. Although the XRD patterns show that the lattice structures of both the foil and LFP part have austenite phase, the high cooling rate of the LFP process forms the metastable austenitic phase, which promotes enhancement of mechanical strength, while the lower cooling rate of the annealed heat treatment process forms the equilibrium austenitic phase.

References

[1] Frazier WE, Polakovics D, Koegel W. Qualifying of metallic materials and structures for aerospace applications. JOM 2001;53:16-18.

[2] Thijs L, Verhaeghe F, Craeghs T, Humbeeck JV, Kruth JP. A study of the microstructural evolution during selective laser melting of Ti-6Al-4V. Acta Materialia 2010;58:3303-3312.

[3] Yap CY, Chua CK, Dong ZL, Liu ZH, Zhang DQ, Loh LE, Sing SL. Review of selective laser melting: materials and applications. 2015;2,041101-21.

[4] Keicher DM, Smugeresky JE, Romero JA, Griffith ML, Harwell LD. Using the laser engineered net shaping (LENS) process to produce complex components from a CAD solid model. Proc. SPIE 2993, Lasers as Tools for Manufacturing II, 1997;91.

[5] Prechtl M, Otto A, Geiger M. Rapid tooling by laminated object manufacturing of metal foil. Advanced Materials Research 2005;6-8:303-312.

[6] Kruth JP, Mercelis P, Van Vaerenbergh J, Froyen L, Rombouts. Binding mechanisms in selective laser sintering and selective laser melting. Rapid Prototyping Journal 2005;11:26-36.

[7] Zhai YW, Lados DA, Brown EJ, Vigilante GN. Fatigue crack growth behavior and microstructural mechanisms in Ti-6Al-4V manufactured by laser engineered net shaping. International Journal of Fatigue 2016;93:51-63.

[8] Li RD, LiuJH, Shi YS, Wang L, Jiang W. Balling behavior of stainless steel and nickel powder during selective laser melting process. International Journal of Advanced Manufacturing Technology 2012;59:1025-1035.

[9] Liu Y, Yang YQ, Mai SZ, Wang D, Song CH. Investigation into spatter behavior during selective laser melting of AISI 316L stainless steel powder. Materials and Design 2015;87:797-806.

[10] Wang L, Pratt P, Felicelli SD, Kadiri HEI, Berry JT, Wang PT, Horstemeyer MF. Pore formation in laser-assisted powder deposition process. Journal of Manufacturing Science and Engineering 2009;131:051008-1-9.

[11] Chen SY, Huang JC, Pan CT, Lin CH, Yang TL, Huang YS, Ou CH, Chen LY, Lin DY, Lin HK, Li TH, Jang JSC, Yang CC. Microstructure and mechanical properties of open-cell porous Ti-6Al-4V fabricated by selective laser melting. Journal of Alloys and Compounds 2017;713:248-254.

[12] Dadbakhsh S, Speirs M, Kruth JP, Humbeeck JV. Influence of SLM on shape memory and compression behaviour of NiTi scaffolds. CIRP Annals-Manufacturing Technology 2015;64:209-212.

[13] Mower TM, Long MJ. Mechanical behavior of additive manufactured, powder-bed laser-fused materials. Material Science and Engineering: A 2016;651:198-213.

[14] Graves RS, Kollie TG, McElroy DL, Gilchrist KE. The thermal conductivity of AISI 304L stainless steel. International Journal of Thermophysics 1991;12:409-415.

[15] Rombouts M, Froyen L, Gusarov AV, Bentefour EH, Glorieux C. Photopyroelectric measurement of thermal conductivity of metallic powders. Journal of Applied Physics 2005;97:024905-1-9

[16] Pujula M, Sanchez-Rodriguez D, Kioez-Olmedo JP, Farjas J, Roura P. Measuring thermal conductivity of powders with differential scanning calorimetry. Journal of Therm Anal Calorim 2016;125:571-577.

[17] Gibson I, Rosen DW, Stucker Brent. Additive Manufacturing Technologies 2010: 207-214.

[18] Prechtl M, Otto A, Geiger M. Laminated object manufacturing of metal foil-process chain and system technology. AMST'05 Advanced Manufacturing Systems and Technology. CISM International Centre for Mechanical Sciences 2005;486.

[19] Chen C, Shen YY, Tsai HL. A foil-based additive manufacturing technology for metal parts. Journal of Manufacturing Science and Engineering 2017;139:024501-1-6.

[20] Kwok CT, Lo KH, Chan WK, Cheng FT, Man HC. Effect of laser surface melting on intergranular corrosion behaviour of aged austenitic and duplex stainless steels. Corrosion Science 2011;53:1581-1591.

[21] Karnati S, Axelsen I, Liou FF, Newkirk JW. Investigation of tensile properties of bulk and SLM fabricated 304L stainless steel using various gage length specimens. Solid Freeform Fabrication Symposium 2016.

[22] Small KB, Englehart DA, Christman TA. Guide to etching specialty alloys. Advanced Materials & Processes 2008;166:32-37.

[23] Griffith ML, Ensz MT, Puskar JD, Robino CV, Brooks JA, Philliber JA, Smugeresky JE, Hofmeister WH. Understanding the microstructure and properties of components fabricated by laser engineered net shaping. Solid Freeform and Additive Fabrication 2000.

[24] Guan K, Wang Z, Gao M, Li X, Zeng X. Effects of processing parameters on tensile properties of selective laser melted 304 stainless steel. Material and Design 2013;50:581-586.

[25] Gil F J, Ginebra MP, Manero JM, Planell JA. Formation of a-Widmanstatten structure: effects of grain size and cooling rate on the Widmanstatten morphologies and on the mechanical properties in Ti6Al4V alloy. Journal of Alloys and Compounds 2001; 329:142-152.

[26] Shen YY, Li YQ, Chen C, Tsai HL. 3D printing of large, complex metallic glass structures. Materials and Design 2017;117:213-222.

[27] Singh KK, Sangal S, Murty GS. Hall-Petch behaviour of 316L austenitic stainless steel at room temperature. Materials Science and Technology 2002;18:165-172.

[28] Forouzan F, Najafizadeh A, Kermanpur A, Hedayati A, Surkialiabad R. Production of nano/submicron grained AISI 304L stainless steel through the martensite reversion process. 2010;527;7334-7339.

[29] Wang ZQ, Palmer TA, Beese AM. Effect of processing parameters on microstructure and tensile properties of austenitic stainless steel 304L made by directed energy deposition additive manufacturing. Acta Materialia 2016;110:226-235.

[30] Hedayati A, Najafizadeh A, Kermanpur A, Forouzan F. The effect of cold rolling regime on microstructure and mechanical properties of AISI 304L stainless steel. Journal of Materials Processing Technology 2010;210:1017-1022.

[31] Fu JW, Yang YS, Guo JJ, Tong WH. Effect of cooling rate on solidification microstructures in AISI 304 stainless steel. Materials Science and Technology 2008;24:941-944.

[32] Mateo A, Zapata A, Fargas G. Improvement of mechanical properties on metastable stainless steels by reversion heat treatments. IOP Conference Series: Material Science Engineering 2013;48:012001.